Personalized Computational Heart Models with T1-Mapped Fibrotic Remodeling Predict Risk of Sudden Death Risk in Patients with Hypertrophic Cardiomyopathy

Ryan P. O'Hara[1], Edem Binka[2], Adityo Prakosa[1], Stefan L. Zimmerman[3], Mark J. Cartoski[4], M. Roselle Abraham[5], Dai-Yin Lu[5], Patrick M. Boyle[6], Natalia A. Trayanova[1*]

[1]Department of Biomedical Engineering, Johns Hopkins University, Baltimore, MD, US. [2]Division of Pediatric Cardiology, Johns Hopkins School of Medicine, Baltimore, MD, US. [3]Department of Radiology, Johns Hopkins School of Medicine, Baltimore, MD, US. [4]Division of Pediatric Cardiology, Nemours/Alfred I. duPont Hospital for Children, Wilmington, DE, US. [5]Division of Cardiology, University of California San Francisco, San Francisco, CA, US. [6]Department of Bioengineering, University of Washington, Seattle, WA, US.

***Correspondence**: Natalia A. Trayanova, 3400 N Charles Street, 216 Hackerman Hall, Baltimore, MD 21218, USA. Tel: +14105164375 | E-mail: ntrayanova@jhu.edu

Competing Interests: The authors declare that no competing interests exist.

Word count excluding Materials and Methods, References, and Figure Legends: 3971

Abstract:

Hypertrophic cardiomyopathy (HCM) causes sudden cardiac death (SCD) due to ventricular arrhythmias (VA) manifesting from myocardial fibrosis proliferation. Current clinical risk stratification criteria inadequately identify at-risk patients in need of primary prevention of VA. Here, we use mechanistic computational modeling of the heart to analyze how HCM-specific remodeling of the heart promotes arrhythmogenesis and to develop a personalized strategy to forecast risk of VAs in these patients. We combine contrast-enhanced cardiac magnetic-resonance (CMR) imaging and T1 mapping data to construct digital replicas of HCM patient hearts that represent the patient-specific distribution of focal and diffuse fibrosis and evaluate the substrate propensity to VA. Our analysis indicates that the presence of diffuse fibrosis, which is rarely assessed in these patients, increases arrhythmogenic propensity. In forecasting future VA events in HCM patients, the imaging-based computational heart approach achieved 84.6%, 76.9%, and 80.1% sensitivity, specificity, and accuracy, respectively, and significantly outperformed current clinical risk predictors. This novel VA risk assessment may have the potential to prevent SCD and help deploy primary prevention appropriately in HCM patients.

Introduction:

Hypertrophic cardiomyopathy (HCM) is the most common cause of sudden cardiac death (SCD) in the young and is a significant cause of sudden death in adults.(Maron, 2004) The disease, with an incidence of 1 in 500, presents with progressive myocardial fibrosis which can create substrates for ventricular arrhythmias (VA) leading to SCD in patients who are typically asymptomatic.(Galati *et al.*, 2016; Olivotto *et al.*, 2012) Implantable cardioverter defibrillator (ICD) deployment, a procedure that carries risk of potential complications and morbidity, is used as primary prevention of SCD due to VA in patients with HCM.(Lambiase *et al.*, 2016; Jayatilleke *et al.*, 2004) However, current risk stratification criteria outlined by the American College of Cardiology Foundation/American Heart Association (ACCF/AHA) and European Society of Cardiology (ESC) fail to accurately identify all patients at risk for SCD, leading to suboptimal rates of appropriate ICD implantation.(Gersh *et al.*, 2011; O'Mahony *et al.*, 2014; Schinkel *et al.*, 2012) Thus, many HCM patients receive ICDs without deriving any health benefits, while others are not adequately protected. Development of accurate means to stratify SCD risk due to VA in HCM patients for guidance of ICD deployment is an important unmet clinical need.

Cardiac magnetic resonance (CMR) imaging with late gadolinium enhancement (LGE) has unparalleled capability in the detection and quantification of scar and dense fibrosis(Prakosa *et al.*, 2014). In HCM, myocardial fibrosis takes the form of both dense (focal) and diffuse fibrosis, with histopathological evidence showing diffuse fibrosis as the hallmark feature of the disease.(Galati *et al.*, 2016) Diffuse fibrosis, however, is not well captured by standard LGE-CMR. Instead, post-contrast T1 mapping, a parametric imaging modality, has been used to visualize diffuse fibrosis in patients with HCM.(Chu *et al.*, 2017; Ellims *et al.*, 2012) We have

previously developed a computational modeling approach (virtual heart) to predict SCD risk due to VA in post-infarction patients,(Arevalo *et al.*, 2016) We hypothesized that a new personalized virtual-heart technology, one that entails constructing fusion electrophysiological models based on the distribution of both dense and diffuse fibrosis, as acquired by the two different CMR modalities, would be predictive of the propensity of the HCM-remodeled substrate to VAs and could thus be used to assess SCD risk due to VA in this patient population.

The goal of this study is to create a personalized virtual-heart approach based on the combination of post-contrast T1 mapping and LGE-CMR and to employ it 1) to analyze how HCM-specific remodeling promotes arrhythmogenesis and 2) in a targeted strategy to forecast risk of VA in HCM patients. In a proof-of-concept patient cohort, we assess the predictive capability of the approach as compared to that of other clinical metrics for VA risk prediction in HCM.

Results:

The new approach to analyzing arrhythmogenic propensity in HCM patients developed here involved creating three-dimensional (3D) patient-specific electrophysiological ventricular models based on fusing data from LGE-CMR and post-contrast T1 mapping. Each model thus represented the personalized distribution of focal fibrosis (scar) and diffuse fibrosis. VA inducibility in each HCM patient's substrate was probed to determine VA risk for the patient and to understand the mechanisms of arrhythmogenesis, and specifically, the contribution of the individualized diffuse fibrosis distribution, which is rarely assessed in these patients. Conceptual overview of our approach to analyzing the arrhythmogenic propensity of HCM patient hearts is presented in Figure 1A.

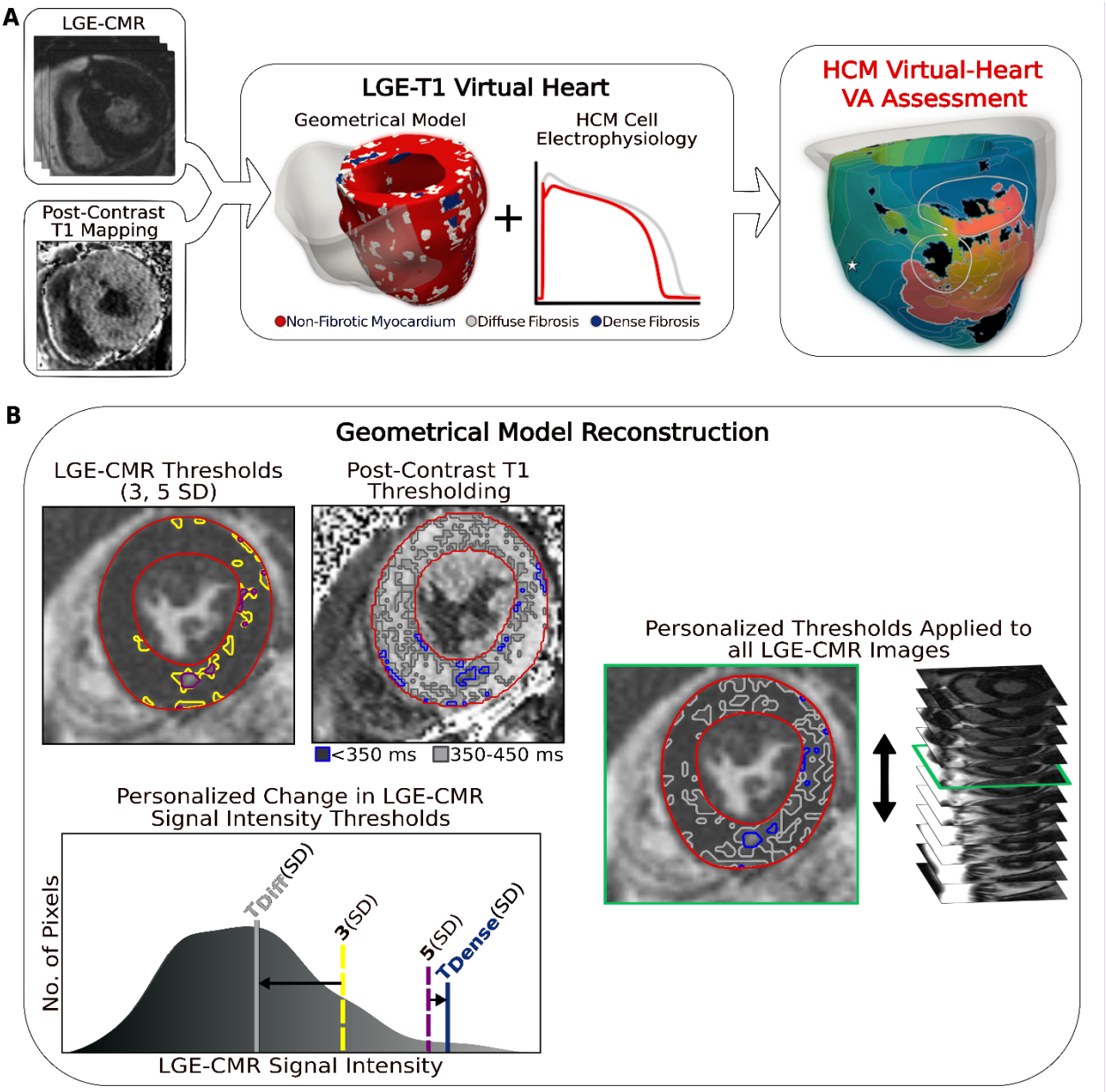

Figure 1. **A.** Flowchart summarizing the virtual-heart VA risk stratification approach for HCM patients. A combination of LGE-CMR and post-contrast T1 mapping is used to construct personalized LV geometrical models with fibrotic remodeling. Incorporating HCM-specific electrophysiological properties (action potential kinetics, conduction velocity) completes the generation of each personalized LGE-T1 virtual heart, which is then used to assess VA propensity in the substrate via rapid pacing. RV is shown in transparent gray. Dense fibrosis

(scar) is considered non-conductive. **B**. Fusing LGE-CMR and post-contrast T1 map information to generate the personalized, geometrical virtual-heart model. Top left: LV segmentation with intermediate and high signal intensity thresholds of 3 (yellow) and 5 SD (purple), respectively, on short-axis LGE-CMR. Bottom left: Mid-ventricular post-contrast T1 map segmentation with relaxation time thresholds of <350 (blue) and 350-450 ms (gray). Right: The thresholds of the LGE-CMR signal intensity were adjusted to new, personalized thresholds, $T_{Diffuse}$ and $T_{Dense,}$ based on the T1 map (see text for detail). D: The new personalized signal intensity thresholds in the matching LGE-CMR slice were then applied to all LGE-CMR short-axis slices.

Patient characteristics:

Twenty-six patients with HCM were included in this study. Demographic information for the cohort is provided in Table 1. All patients were adults (median age 53 years) and our cohort was 19% female. Thirteen of the 26 HCM patients experienced clinical VAs. Of the clinical parameters that associate with SCD in HCM (FHSCD, unexplained syncope, MWT, Max LVOTG, Age, LA diameter; see Table 1 for abbreviations), there were no statistically significant differences (*P = 0.34, -, 0.65, 0.72, 0.98, 0.26*) between patients with and without clinical VA. There was no statistically significant difference in any of the other common clinical characteristics between the two groups. Clinical data alone was not sufficient to accurately determine VA risk in this population.

Table 1. Patient Characteristics (N=26)

Clinical Characteristic	Patients without VA, n=13	Patients with VA, n=13	*P* value
Male	12 (92)	9 (69)	0.08
Age at CMR, years	49.7 [19-76]	49.8 [22-78]	0.98
NYHA III/IV	4 (31)	4 (31)	-
Myectomy	1 (8)	1 (8)	-
ASA	1 (8)	2 (15)	0.34
Amiodarone	0 (0)	1 (8)	0.34
Persistent AF	3 (23)	4 (31)	0.34
LA Diameter, mm	43.8 ± 6.3	38.3 ± 12.7	0.26
Max LVOTG, mmHg	57.8 [4-154]	50.8 [8-160]	0.72
MWT, mm	20.5 ± 5.0	19.6 ± 5.6	0.65
FS, %	38.0 ± 10.2	40.3 ± 10.8	0.40
FHSCD	3 (23)	4 (31)	0.34
Unexplained Syncope	3 (23)	3 (23)	-

Values are given as n (%), mean [range], or mean ± SD. P values were calculated using Student *t* test (P≤.05 considered statistically significant). VA=ventricular arrhythmia; CMR=cardiac magnetic resonance; ASA=alcohol septal ablation; AF=atrial fibrillation; LA=left atrium; LVOTG=left ventricular outflow tract gradient; MWT=maximum wall thickness; FS=fractional shortening; FHSCD=family history of sudden cardiac death.

Assessment of HCM Structural Remodeling Using LGE-T1 Geometrical Models:

To reconstruct the geometrical model of each patient's heart, LGE-CMR and post-contrast T1 mapping images were combined, creating a personalized LGE-T1 fusion model of HCM ventricular geometry and structural remodeling. Figure 1B presents the "fusing" process, in which an initial reconstruction of ventricular geometry and scar/fibrosis was performed from

the LGE-CMR images using standard "one-size-fits-all" thresholds, and then the relaxation times from the short-axis T1 map were used to define *personalized* signal intensity thresholds to delineate areas of diffuse fibrosis and scar (see Methods for detailed description). The personalized thresholds were unique to each patient. The additional personalization of the geometrical model furnished by the usage of the T1 mapping data ensured a comprehensive representation of the individualized structural remodeling in each patient heart.

Once the geometrical models were reconstructed, they were analyzed to determine whether the level (amount) and/or distribution of structural remodeling discriminate between patients with and without clinical VA. The level of regional hypertrophy was first assessed, as measured by the wall thickness of the heart models. No statistically significant difference in regional hypertrophy was found at the septum (*P=0.61*), anterior wall (*P=0.84*), posterior wall *(P=0.94*), and apex (*P=0.73*) between heart models of patients with and without clinical VA, as shown in Table 2. These results indicated that the level of hypertrophy does not discriminate between arrhythmogenic and non-arrhythmogenic substrates in HCM patients.

Table 2. LV wall thickness in HCM patients with and without clinical VA

	Patients without VA, n=13	**Patients with VA, n=13**	***P* value**
Wall Thickness (mean ± SD)			
Septum, mm	11.3 ± 8.4	13.1 ± 9.2	0.61
Anterior, mm	11.3 ± 7.4	10.7 ± 7.3	0.84
Posterior, mm	11.1 ± 7.2	11.3 ± 7.3	0.94
Apex, mm	7.9 ± 5.3	7.2 ± 4.8	0.73

P values were calculated using Student *t* test (P≤.05 considered statistically significant).

Figure 2A and B presents a comparison between geometrical heart models of 2 patients (one with clinical VA and another without) reconstructed by combining LGE-CMR with T1 mapping, and by using LGE-CMR only. In the latter models, the accepted "one-size-fits-all" thresholds of 3 and 5 times the standard deviation (SD) of the low-intensity mean were used to reconstruct dense fibrosis (scar) and diffuse fibrosis distributions (see Methods). In the former models, patient-specific thresholds from the T1 mapping were used to delineate dense and diffuse fibrosis. As evident from the figure, using patient-specific signal intensity thresholding from the T1 map resulted in a significantly higher amount of diffuse fibrosis in these two models (42.9 ± 3.4% vs 9.8 ± 0.1%).

For all HCM LGE-T1 fusion models, the average threshold for diffuse fibrosis, $T_{Diffuse}$, was 1.1 ± 0.7, significantly different from the corresponding LGE "one-size-fits-all value", 3 SD. The average threshold for dense fibrosis, T_{Dense}, was 5.1 ± 0.5, not a significant change from the original 5 SD. The personalized threshold adjustment did not therefore result in a significant change in the amount of dense fibrosis for LGE-T1 models compared to LGE-only models (averages of 3.8 ± 2.3 vs 3.2 ± 1.3, *P=0.30*). However, it resulted in a significant change in diffuse fibrosis across all models, as illustrated in Fig. 2C (40.5 ± 9.4% for LGE-T1 vs 8.9 ± 1.7% for LGE only, *P<0.0001*).

No statistical differences were found in the amounts of diffuse fibrosis between LGE-T1 models with and without clinical VA (P=0.53, confidence interval; CI: [36.8 44]) and between LGE-only models with and without clinical VA (P=0.94, CI: [8.25 9.53]; Fig.1B); also, no statistical difference was found in the amount of scar (3.7 ± 2.2% vs 3.8 ± 2.5, *P=0.91* for LGE-T1 and 3.4 ± 1.2% vs 3.0 ± 1.5%, *P=0.53* for LGE only models). These results indicate that the imaging characteristics of HCM structural remodeling, as visualized by the combination of LGE-

CMR and T1 mapping, cannot be used to discriminate between patients who will and will not develop clinical VA.

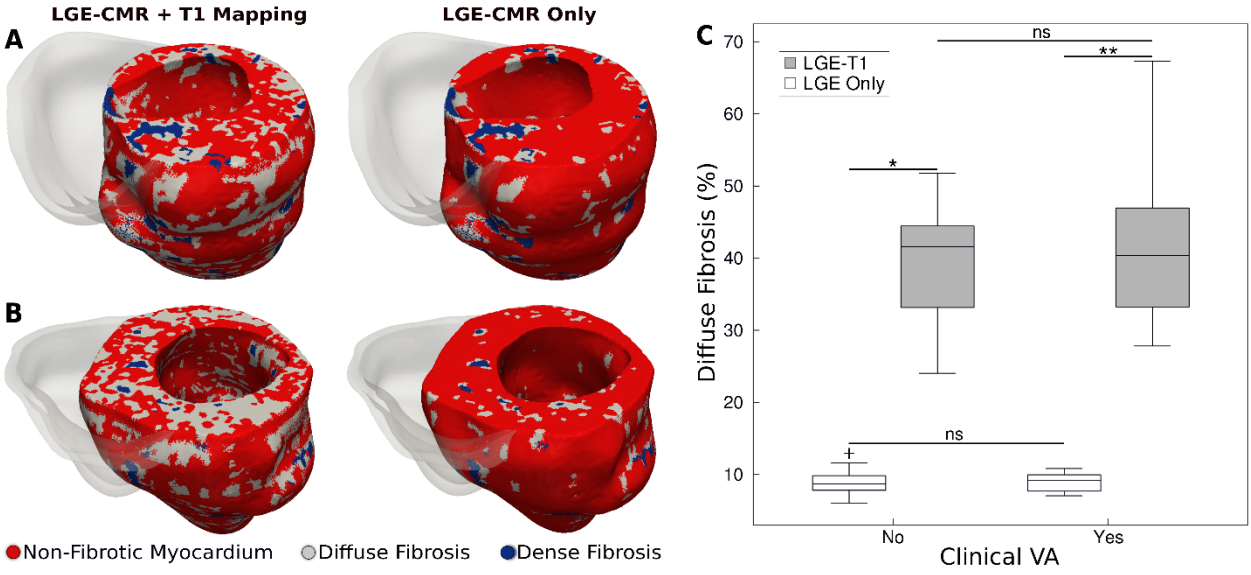

Figure 2. **A and B**. Examples of HCM personalized LV geometrical models with fibrotic remodeling (RV shown in transparent gray) reconstructed using LGE-CMR images with personalized T1-informed fibrosis segmentation thresholds (left) and using LGE-CMR images with one-size-fits-all fibrosis segmentation thresholds of 3 and 5 SD (right). There is significantly more diffuse fibrosis in the T1-adjusted models. **A**: Heart model from an HCM patient without clinical VA. **B**: Heart model from an HCM patient with clinical VA. **C**. Boxplot of the amount of diffuse fibrosis in LGE-T1 and LGE-only HCM geometrical models without clinical VA (LGE-T1: N=13, IQR=12.54; LGE Only: N=13, IQR=2.41; *P<0.0001) and with clinical VA ((LGE-T1: N=13, IQR=14.44; LGE Only: N=13, IQR=2.46; **P<0.0001).

Figure 2 – source data 1; Spreadsheet including source data underlying Figure 2.

For each geometrical model used in this study, the amount of diffuse fibrosis in each LGE-T1 and LGE only model. Figure2_SourceData.xlsx

178

179 **Assessment of Propensity to VA in HCM LGE-T1 Virtual Heart Models**

180 Once the geometrical models of all HCM patients were reconstructed, electrophysiologi-
181 cal models were generated and used to assess the individualized propensity to VA by pacing from
182 distributed ventricular sites, representing potential ectopy. Full detail is in Methods. A total of
183 182 simulations ([26 patient heart] x [7 pacing locations]) were performed to probe propensity to
184 VA induction in this cohort. To be able to better understand the role of T1-based diffuse fibrosis
185 in arrhythmogenesis, we also repeated the simulations with LGE-only models.

186 Figure 3 presents reentrant arrhythmias induced (from sites marked with stars) in 3 LGE-
187 T1 virtual hearts from patients with known clinical VAs. In all three cases, a single VA morphol-
188 ogy was induced. In Figure 3, left, the VA localized in a region of interdigitated diffuse and dense
189 fibrosis. In Figure 3 middle, there was a figure-of-eight reentry in a transmural region of diffuse
190 fibrosis. In Figure 3 right, the VA shown was induced from two different pacing sites, one in the
191 basal lateral and another in the inferoseptal wall and persisted also in a region of interdigitated
192 diffuse and dense fibrosis.

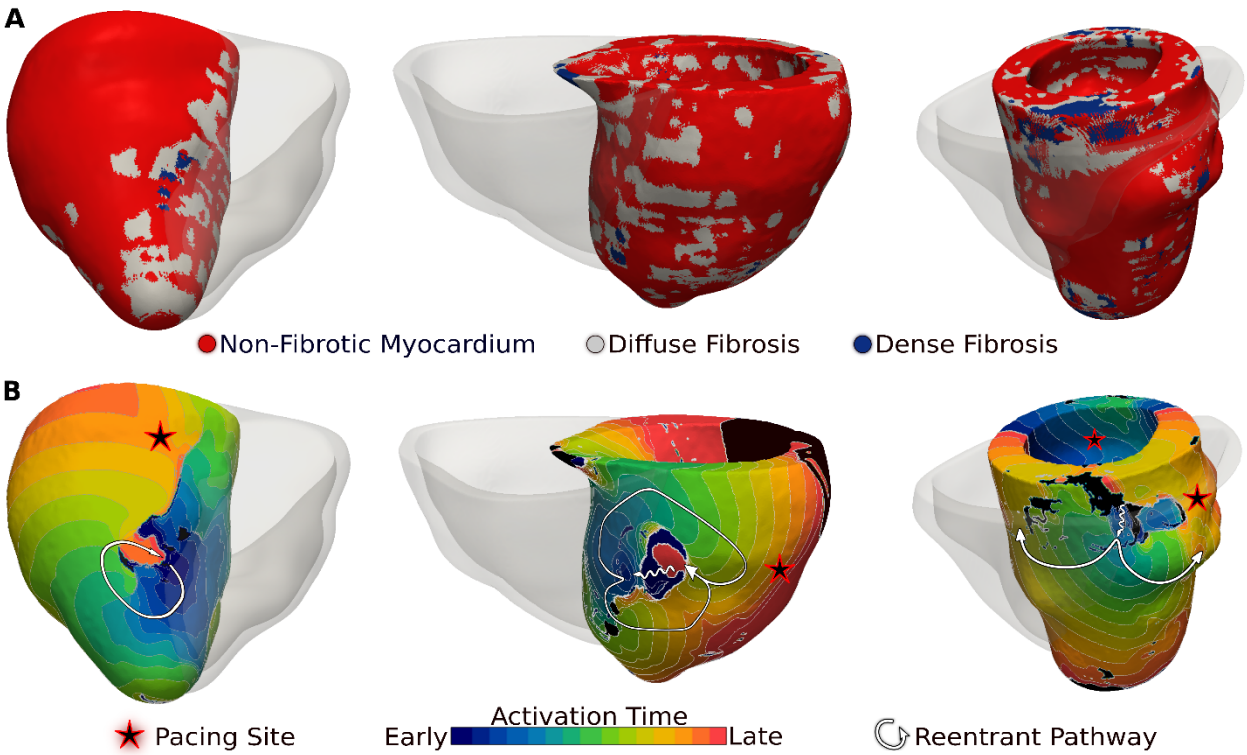

193

194 **Figure 3**. VAs induced in 3 LGE-T1 virtual hearts from patients with known clinical VAs. **A**.

195 Reconstructed patient-specific geometrical models. **B**. Activation patterns of the reentry induced

196 from the pacing site(s) marked with star. Black regions did not activate during the timeframe

197 shown.

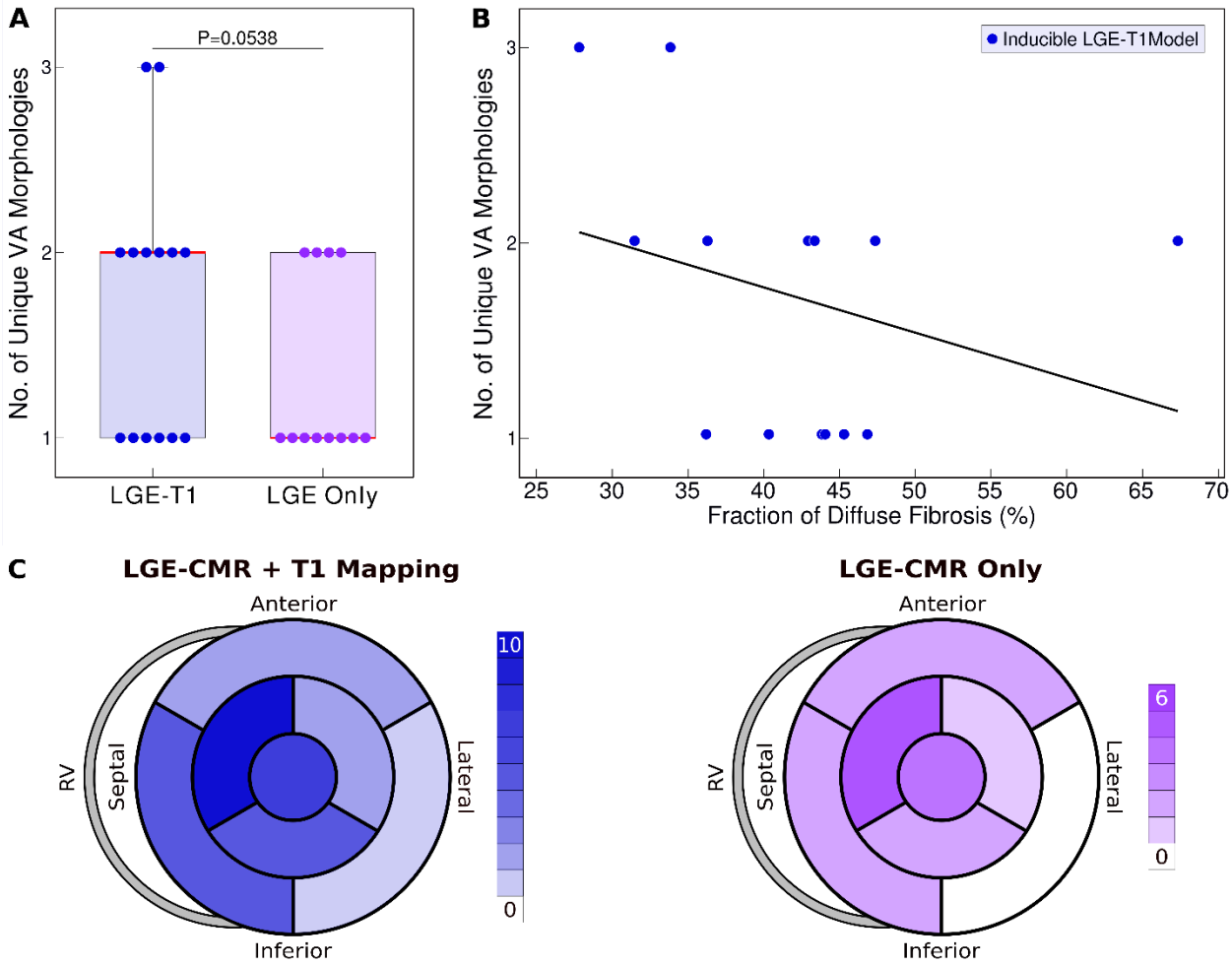

Figure 4. Relationship between T1-based diffuse fibrosis and VA inducibility in LGE-T1 and LGE-only personalized virtual heart models of HCM patients. **A.** Comparison of the number of unique VA morphologies between inducible LGE-T1 and LGE-only models for all VA-inducing pacing sites. (LGE-T1: N=14, IQR=1; LGE Only: N=12, IQR=0.75; P=0.0538, CI [1.25, 1.75]) **B.** Correlation between amount of T1-based diffuse fibrosis and the number of unique VA morphologies induced in LGE-T1 models (R=-0. 3048, P=0.289). **C.** Distribution of the pacing sites that induced VAs in LGE-T1 and LGE-only models.

Figure 4 – source data 1; Spreadsheet including source data underlying Figure 4.

For each geometrical model that reentry was induced, the number of unique VA morphologies and amount of diffuse fibrosis in each LGE-T1 and LGE only model. Figure4_SourceData.xlsx

Of the 26 LGE-T1 models, 14 were found inducible for VA in simulations. In contrast, only 12 LGE-only models were found inducible, indicating that the presence of diffuse fibrosis leads to increased VA inducibility. Figures 4 and 5 explore the mechanistic contributions to increased VA vulnerability in models with T1-based diffuse fibrosis.

Fig. 4A presents the number of unique VA morphologies induced by the pacing protocol. LGE-T1 models had a total of 24 unique VAs induced in them (out of total 32 VA episodes induced in the LGE-T1 models); in each model, there were between 1 and 3 different VA morphologies. LGE-only models had a total of 15 unique VAs (with a total of 17 VA episodes induced in these models), with only 1 or 2 distinct VA morphologies induced per model. These results indicate that the presence of diffuse fibrosis as reconstructed from T1 mapping increases the number of unique VAs in each substrate. Fig.4B correlates the amount of diffuse fibrosis and the number of unique VAs ($R=-0.3048$, $P=0.289$) in LGE-T1 inducible models. The moderate negative correlation indicates that the distribution of diffuse fibrosis is more important than its amount as the mechanism of VA inducibility in the HCM-remodeled substrate. Figure 4C presents two bullseye plots with the 7 AHA regions in which pacing sites were located; shown are the number of pacing sites in each segment that elicited VAs in LGE-T1 and LGE-only inducible models. In the LGE-T1 models, out of the 98 pacing sites (7 pacing sites per each of the 14 inducible models), 32 (33%) resulted in VA induction. In contrast, out of 84 pacing sites in the 12 LGE-only inducible models, 17 (20%) resulted in VA induction. Thus, the presence of T1-based diffuse fibrosis renders the substrate inducible from a larger number of ectopic locations, contributing to the overall increased vulnerability to VA. Interestingly, the sector with the pacing sites that induced most VAs (mid anteroseptal) and that with least (basal inferolateral) were the same in LGE-T1

and LGE-only models, indicating that the additional T1-based diffuse fibrosis localizes to the sectors with arrhythmogenic substrate in the LGE-only models. Overall, the distribution of pacing sites is the same (with small exception in the basal regions), but the number of sites per sector increased with the presence of diffuse fibrosis.

Figure 5 explores the contribution of T1-based diffuse fibrosis to VA inducibility by comparing arrhythmogenesis in individual models. Panel A shows, for the 13 patients with clinical VAs, the number of distinct VAs per patient model. First, LGE-T1 modeling documented correctly VA occurrence in the digital substrates of 11 of the 13 patients with clinical VAs (compared to 9 LGE-only correct VA predictions); thus, the representation of T1-based diffuse fibroses increased the fidelity of the HCM virtual heart approach. Second, while the number of unique VA morphologies per inducible virtual heart increased in LGE-T1 models as compared to LGE-only (consistent with data in Fig. 4A), with LGE-T1 models having maximum 3 unique VAs (vs. 2 in LGE-only) in the cohort, this plot points to interesting VA dynamics in individual substrates. Patients 5, 6, and 9 had the same level of arrhythmogenicity of the substrate (1 VA induced) regardless of the presence of T1-based diffuse fibrosis. An example of VA dynamics in these models is shown in Fig.5B (patient 6). The additional diffuse fibrosis did not alter the location or direction of VA reentry; the reentry occurred in a region of dense scar in both types of models. Although the T1-based diffuse fibrosis (36.2%) in this patient augments the existing diffuse fibrosis of the LGE-only model (9.6%), there are no additional VA morphologies. However, the activation dynamics were altered, with propagation being less organized.

In the reminder of the clinical-VA patients in Fig. 5A, the presence of T1-based diffuse fibrosis resulted in the occurrence of additional VA(s), on top of that (those) also present in the LGE-only model. Furthermore, there was not a strict correspondence between the VAs in the

LGE-only models and the equivalent ones in the LGE-T1 virtual heart in terms of VA locations and dynamics. This indicates that the arrhythmogenic substrate changes in a global fashion when T1-based diffuse fibrosis in considered. An example is presented in Fig. 5C (patient 9).

As VAs in HCM patients can occur under different circumstances and be documented by different means, there is no invasive clinical mapping data for these patients regarding the location and morphologies of the clinical VAs. However, two patients in this cohort underwent clinical electrophysiology studies that identified episodes of VA. The simulated VAs in the LGE-T1 models matched the locations of the clinical VAs as documented by the chart review.

It remains unclear why patients 1 and 2 had non-inducible LGE-T1 substrates despite having clinical VAs. The amount of diffuse fibrosis in these 2 substrates (42.4 ± 12.2%) was similar to that in the 11 inducible substrates (41.2 ± 10.9%); similar was the finding regarding dense scar. Additionally, the maximum wall thickness and the thickness distribution fall into the same ranges as the averages of the cohort. It is possible that there have been other factors, including electrophysiological remodeling that the fusion substrate-based modeling approach presented here cannot capture. Despite incorrect prediction in 2 out of 26 patients in the HCM cohort, the VA risk prediction capabilities of the LGE-T1 virtual-heart approach significantly surpassed those of any current clinical risk assessment approaches, as detailed in the next section.

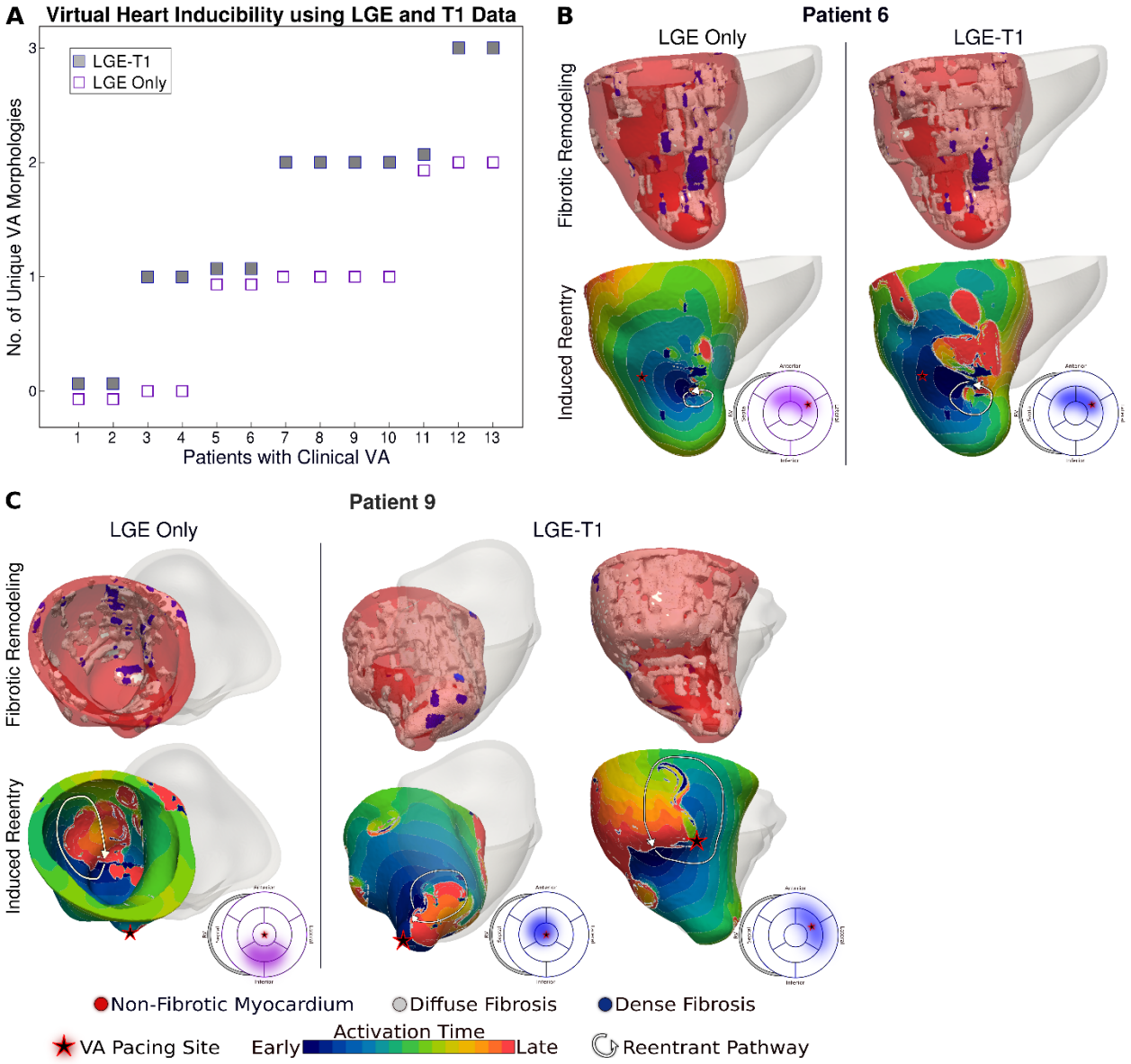

Figure 5. Comparison of arrhythmogenesis in HCM models of patients with clinical VAs. **A**: Plot of the number of unique VA morphologies for patients with clinical VA using LGE-T1 LGE-only models. **B and C**: Comparison of VAs in corresponding LGE-T1 and LGE-only models. Pacing site(s) are marked with stars. Bullseye plots show the pacing site location (star) and the location of the reentrant pathway in LGE-T1 (blue) and LGE-only (purple) models.

Figure 5 – source data 1; Spreadsheet including source data underlying Figure 5.

For each geometrical model with clinical VA, the number of unique VA morphologies in each LGE-T1 and LGE only model. Figure5_SourceData.xlsx

Assessment of the Capability of the HCM Virtual Heart VA Risk Prediction:

After examining the mechanistic underpinning of arrhythmogenesis and the role of T1-based diffuse fibrosis in the HCM substrate, we conducted a comparison of our VA risk predictor capability with the clinical risk assessment guidelines of the American College of Cardiology Foundation (ACCF)/American Heart Association (AHA) and European Society of Cardiology (ESC). Results are presented in Table 3, illustrating that both existing clinical approaches were significantly inferior in predicting VA risk in this cohort. Of the 13 HCM patients with clinical VAs, the ACCF/AHA model predicted correctly 6 of the patients, while the ESC model predicted correctly 7 patients; the LGE-T1 virtual heart approach predicted correctly 11 patients. Overall, our LGE-T1 virtual heart technology exhibited higher accuracy and greater sensitivity and specificity (80.1%, 84.6%, and 76.9%) as compared to the best performing corresponding metrics of the clinical risk assessment methodologies (46.2%, 53.9%, and 46.2% for accuracy, sensitivity, and specificity).

For completeness, data at the bottom of Table 3 quantifies the predictive capability of the substrate arrhythmogenesis approach when using LGE-only models (9 patients predicted correctly out of 13). Interestingly, even without the additional T1 personalization (i.e. without accounting for T1-based diffuse fibrosis), the LGE-only virtual-heart technology outperformed the clinical risk stratifiers in this HCM cohort. This finding indicates that assessing the arrhythmogenic propensity of the substrate is of paramount importance to HCM VA risk stratification, even when the distribution of diffuse fibrosis may not be accurately represented.

Table 3. Predictive Capability of HCM Virtual-Heart Technology

	Sensitivity	Specificity	PPV	NPV	Accuracy
ACCF/AHA Risk Model	**46.2**	**46.2**	**46.2**	**46.2**	**46.2**
ESC Risk Model	**53.9**	**38.5**	**46.7**	**45.5**	**46.2**
Virtual Heart Technology: LGE-T1	**84.6**	**76.9**	**78.8**	**83.3**	**80.1**
Virtual Heart Technology: LGE Only	**69.2**	**76.9**	**75.0**	**71.4**	**73.1**

ACCF=American College of Cardiology Foundation, AHA=American Heart Association, ESC=European Society of Cardiology.

Discussion:

In this study, we presented a new personalized virtual heart approach for assessing arrhythmia risk in patients with HCM, which could be used in guiding clinical decisions for prophylactic ICD implantation. Our technology uses multiscale computational models of patients' hearts reconstructed on the basic of the fusion of imaging data from LGE-CMR and T1 mapping. With the inclusion of information from post-contrast T1 mapping, a quantitative and parametric imaging modality, extensive diffuse fibrotic remodeling, which is a hallmark of HCM, is adequately represented. Here, this is done by adjusting the diffuse fibrosis intensity-based thresholds in model construction based on the T1 maps, while preserving the identification of dense scar from LGE-MRI. These are the first personalized heart models created with data from different types of CMR; previous personalized modeling approaches for VA assessment have utilized LGE-MRI scans in reconstructing model geometry/structure(Prakosa *et al.*, 2014; Cartoski *et al.*, 2019; Arevalo *et al.*, 2016). Once constructed, the mechanistic personalized electrophysiological models were used to analyze how HCM-induced remodeling, and

specifically the presence of diffuse fibrosis promotes arrhythmogenesis. Finally, the capability of our approach to forecast future VA events was assessed in the cohort of 26 HCM patients.

Presence of diffuse fibrosis has been suggested previously as a potential factor in increased risk of VA, in addition to focal scar. Previous studies have found associations between diffuse fibrosis and VA in non-ischemic dilated cardiomyopathies(Nakamori *et al.*, 2018) and mitral valve prolapse(Bui *et al.*, 2017). Additionally, diffuse ventricular fibrosis has been found to increase left atrial pressure, and may be a marker of atrial fibrillation recurrence post-ablation(Begg *et al.*, 2020). However, its contribution to arrhythmogenic propensity in HCM patients has never been assessed before. This study found that the presence of T1-based diffuse fibrosis resulted in the occurrence of new VAs, in addition to those arising from scar (as assessed by signal heterogeneities in LGE-MRI). Furthermore, T1-based diffuse fibrosis distribution rendered the substrate inducible from a larger number of ectopic locations, contributing to the overall increased vulnerability to VA.

In this retrospective proof-of-concept HCM study, the personalized LGE-T1 virtual heart technology demonstrated excellent performance in forecasting future VA events in HCM patients, achieving 84.6%, 76.9%, and 80.1% sensitivity, specificity, and accuracy, respectively. It outperformed both risk models used in current clinical practice, the ACCF/AHA and ESC models. Indeed, all 26 HCM patients in our study were deemed at high risk for SCD by the ACCF/AHA criteria and received ICDs for primary prevention, but only 13 patients, i.e. 50% of the cohort, actually experienced VA (appropriate ICD firing). Should our LGE-T1 virtual heart technology be proven to be a superior risk predictor in larger clinical studies, it would advance the management of patients with this complex disease, helping to ensure that those at high risk

for VA are adequately protected by ICDs and that unnecessary ICD implantations and the associated device complications are minimized.

The HCM virtual-heart technology's ability to comprehensively evaluate substrate arrhythmogenicity, as probed by rapid pacing delivered at a number of uniformly-distributed ventricular locations, is paramount to its superior performance. Even when using only LGE-CMR in model construction, which reliably detects focal scar (dense fibrosis) but underestimates the amount of non-ischemic fibrotic remodeling, our technology still offers VA risk assessment that is superior to the clinical risk models. However, the use of T1 maps in model construction confers a higher level of personalization in each patient heart model as compared to LGE only (i.e. personalized thresholds for segmentation), which ultimately translates into superior predictive capability.

HCM is a genetic disease that progresses throughout the life of the patient, and a cardiac event might be a phenotypic expression of the disease at any point of time. Therefore, we envision that in the clinical application of our technology, patients would be re-imaged at different time points and risk assessment repeated to account for changes in arrhythmia susceptibility over time as the diseased heart remodels.

The technology developed here charts a new direction in the use of biophysically-detailed heart modeling in the prognosis of rhythm disorders. A number of different imaging modalities used in patient assessment such as positron emission tomography (PET) or single-photon emission computerized tomography (SPECT) could also be integrated with LGE-CMR to construct hybrid heart computational models. Combining such computational approaches with machine learning techniques(Shade *et al.*, 2020a; Shade *et al.*, 2021) will enable the incorporation of additional patient clinical data, such as genetic information, phenotypic

367 characterization, as well as time series, such as electrocardiography (ECG), in the diagnosis and
368 treatment of complex cardiac diseases.
369
370 **Study Limitations:**
371 Our study has a small sample size, limited by the fact that a number of LGE-CMR scans
372 of HCM patients had imaging artifact, which prevented us from reconstructing a larger number
373 of virtual hearts. Specifically, aliasing and motion artifacts were main causes for excluding
374 patient data as well as incomplete scans (operator did not scan the entire LV). Further, in some
375 patients there were discrepancies between the post-contrast T1 map and the matching LGE-CMR
376 short axis scan as the in-plane resolution and slice thickness. However, these discrepancies were
377 mitigated by binning the regions of fibrotic remodeling and electrophysiogical changes instead of
378 using a continuum.
379
380 **Methods:**
381 **Study Overview**:
382 The methodology for assessing VA risk in HCM patients involves creating three-
383 dimensional (3D) patient-specific electrophysiological ventricular models with data from LGE-
384 CMR and post-contrast T1 mapping. Each model represents the personalized distribution of both
385 focal fibrosis (scar) and diffuse fibrosis, both of which contribute to the formation of the
386 arrhythmogenic substrate. VA inducibility in each HCM patient's substrate is probed to
387 understand the mechanisms of arrhythmogenesis, and specifically the contributions to it of the
388 focal and diffuse fibrosis distributions, and to determine VA risk for the patient. Conceptual
389 overview is presented in Figure 1.

The predictive capabilities of the virtual-heart HCM VA risk stratifier were evaluated retrospectively in a proof-of-concept study using data from 26 HCM patients. We chose a cohort that was balanced between patients with VAs based on appropriate ICD firings (13 patients) and without arrhythmic events (the other 13 patients). All patients underwent implantation of clinically indicated ICDs. Virtual-heart predictions of VA risk, executed blindly, were compared to clinical outcomes.

Study Population:

The 26 patients were diagnosed with HCM based on the presence of left-ventricular (LV) wall thickness ≥15 mm on 2-dimensional echocardiography in the absence of other ventricular diseases, including hypertrophy of the right ventricle (RV), between 2011 and 2016 at Johns Hopkins Hospital.(Chu *et al.*, 2017) All patients were clinically referred for prophylactic ICD implantation, being deemed at high risk for VA based on clinician assessment. T1 maps and LGE-CMR were obtained pre-ICD implantation. Patients were followed for the primary end point of appropriate ICD firing due to VA. As stated above, of the 26 HCM patients, 13 (50%) had known VA episodes based on appropriate ICD firing. Patient clinical characteristics are shown in Table 1.

Imaging Data:

Patients whose imaging data was retrospectively used in this study had cardiac CMR examinations using a 1.5-T scanner (MAGNETOM Avanto; Siemens Healthcare, Erlangen, Germany) prior to ICD implantation. Short-axis LGE-CMR images were acquired as previously described.(Chu *et al.*, 2017) In addition, a single mid-ventricular short-axis post-contrast T1 map

was acquired 25 minutes after gadolinium injection using a MOLLI sequence.(Chu *et al.*, 2017) All patient imaging data for model generation was obtained under IRB approval.

Geometrical Reconstruction of Patients' Hearts from T1 Maps and LGE-CMR Images:

In generating HCM patients' virtual hearts, a geometrical model of each patient's heart was first reconstructed by combining the patient's LGE-CMR and post-contrast T1 mapping images. The LV myocardium was segmented from short-axis LGE-CMR as previously described.(Arevalo *et al.*, 2016) The RV was not reconstructed due to blood pool artifacts and the lack of hypertrophy and fibrotic substrate in HCM patients. The LGE-CMR was processed in the standard manner for reconstructing LV geometrical models of patients with ischemic(Arevalo *et al.*, 2016) or non-ischemic cardiomyopathy,(Shade *et al.*, 2020b; Cartoski *et al.*, 2019) which incorporate the distribution of scar and surrounding gray (border) zone. Specifically, as LGE-CMR is an image of relative intensity, the mean of the low signal intensity region in each image was determined, the latter representing myocardium without detectable fibrosis. The standard deviation (SD) of that mean value was used to threshold regions of intermediate (>3 SD above the mean) and high (>5 SD above the mean) signal intensity in the LV, representing fibrotic gray zone and focal scar. Figure 1B, top left, shows these thresholds applied to one LGE-CMR image. The same SD thresholds were used for all models.

Information from the patient's post-contrast T1 mapping was next incorporated in each geometrical heart model. As only a single short-axis mid-LV post-contrast T1 map (Fig.1B) was acquired for each patient, the matching slice (Fig.1B, top left) in the LGE-CMR stack was first found. The relaxation times from the short-axis T1 map were used to define new, *personalized* signal intensity thresholds (different from the "one-size-fits-all" thresholds of 3 and 5 SD of the

low-intensity mean) to delineate areas of intermediate and high signal intensities in the corresponding LGE slice. Specifically, regions in the LGE-CMR slice corresponding to short (<350ms) and intermediate (350-450ms) relaxation times in the T1 map were thresholded (Fig.1B). Based on evidence in histopathological studies(Ellims *et al.*, 2012; Iles *et al.*, 2008; Mewton *et al.*, 2011; Ellims *et al.*, 2014), these regions in the T1 map represent dense fibrosis (scar) and diffuse fibrosis.

The thresholds in the LGE-CMR slice, originally 3 and 5 SD of the mean signal intensity of the normal myocardium, were changed to new values ($T_{Diffuse}$ and T_{Dense}, in units of SD, Fig.1B, bottom left) such that the amount and distribution of tissue of mid- and high signal intensity in the LGE-CMR slice matched those in the T1 map. The new personalized signal intensity thresholds in the matching LGE-CMR slice were then applied to all LGE-CMR short-axis slices (Fig.1B, right) for the given patient to complete the generation of the LGE-T1 geometrical heart model (Fig.1A, middle); the personalized thresholds were unique to each patient. Using T1 mapping provided additional personalization of the model geometrical reconstruction and ensured a comprehensive representation of the individualized structural remodeling in each patient heart.

High resolution finite-element tetrahedral meshes, with an average resolution of 355 ± 69 μm, were constructed directly from the ventricular segmentations using finite element analysis software (Mimics Innovation Suite; Materialise, Leuven, Belgium). Fiber orientations were applied to each mesh using a previously validated approach.(Bayer *et al.*, 2012; Prassl *et al.*, 2009)

Electrophysiological Properties in the HCM Virtual Hearts:

459 The personalized 3D virtual hearts of HCM patients incorporated electrical functions
460 from the cellular scale to the whole heart. Electrophysiological remodeling was incorporated in
461 each virtual heart based on the reconstruction of heterogeneously distributed structural
462 remodeling.

463 At the cellular level, in regions of non-fibrotic myocardium, the human ventricular
464 myocyte model by ten Tusscher et al(ten Tusscher and Panfilov, 2006) was used, with added
465 representation of I_{NaL}(O'Hara *et al.*, 2011), as done in our previous studies.(Shade *et al.*, 2020b;
466 Cartoski *et al.*, 2019; Arevalo *et al.*, 2016; Prakosa *et al.*, 2018) For regions of diffuse fibrosis,
467 we modified the ionic conductances of the ten Tusscher model based on data reported by Coppini
468 et al.(Coppini *et al.*, 2013) In the latter study, prolonged action potential duration and notch
469 elevation following depolarization were observed in experimental recordings from myocytes in
470 hyperthrophied regions acquired via myectomy. As regions of hypertrophy in the HCM heart are
471 also characterized with diffuse fibrotic remodeling, as per histopathological evidence,(Galati *et*
472 *al.*, 2016) in the absence of experimental reports of specific ionic changes in regions of diffuse
473 fibrosis, we used those reported by Coppini et al.(Coppini *et al.*, 2013) Figure 1A, middle, shows
474 the action potentials implemented in regions of fibrotic and non-fibrotic myocardium.

475 At the tissue level, conductivity values along the longitudinal and transverse fiber
476 directions in fibrotic and non-fibrotic myocardium were the same as previously implemented for
477 non-ischemic patient heart models.(Shade *et al.*, 2020b) Dense fibrosis was considered
478 electrically inexcitable. Once completed, the patient-specific HCM electrophysiological heart
479 models were used to assess the patient's risk of arrhythmia.

480

481 **Assessing VA Risk in the Personalized HCM Computational Models**:

Full details regarding the simulation of electrical activity in the virtual hearts can be found in previous publications.(Plank *et al.*, 2008; Prakosa *et al.*, 2018; Vigmond *et al.*, 2008) Briefly, these were finite element heart models, where simulation of electrical activity was performed in a monodomain representation of the myocardium using the software package CARP (https://carp.medunigraz.at/). Each virtual heart was paced sequentially from seven uniformly distributed endocardial LV locations using a validated rapid pacing protocol described in detail in previous studies.(Prakosa *et al.*, 2018; Arevalo *et al.*, 2016; Cartoski *et al.*, 2019) Similar to our work on VA risk stratifications for patients with ischemic cardiomyopathy,(Arevalo *et al.*, 2016) simulation results were analyzed to determine whether reentrant VA was induced in the LV HCM models following rapid pacing from any of the sites. If VA was induced from at least one pacing site in a given personalized HCM virtual heart, the patient was then considered at risk of VA. Simulation results were blind to clinical outcome.

The capability of our HCM virtual heart technology to predict VA risk was compared to risk scores for prophylactic ICD implantation developed by ACCF/AHA(Gersh *et al.*, 2011) and ESC(O'Mahony *et al.*, 2014) using the patient clinical data.

Funding:

This work was supported by NIH grants R01HL142496 and R01HL126802 to N.T., a grant from the Leducq Foundation to N.T., an NIH T32 Fellowship (HL125239) to E.B., and a National Science Foundation Graduate Research Fellowship (DGE-1746891) to R.O.

Acknowledgments:

The authors are grateful to Dr. Iacoppo Olivotto from Careggi University Hospital, Florence, Italy, for the inspiration and discussions.

Disclosures:

None.

References:

Arevalo, H. J., Vadakkumpadan, F., Guallar, E., Jebb, A., Malamas, P., Wu, K. C. and Trayanova, N. A. (2016) 'Arrhythmia risk stratification of patients after myocardial infarction using personalized heart models', *Nat Commun,* 7, pp. 11437.

Bayer, J. D., Blake, R. C., Plank, G. and Trayanova, N. A. (2012) 'A novel rule-based algorithm for assigning myocardial fiber orientation to computational heart models', *Ann Biomed En,* 40(10), pp. 2243-2254.

Begg, G. A., Swoboda, P. P., Karim, R., Oesterlein, T., Rhode, K., Holden, A. V., Greenwood, J. P., Shantsila, E., Lip, G. Y. H., Plein, S. and Tayebjee, M. H. (2020) 'Imaging, biomarker and invasive assessment of diffuse left ventricular myocardial fibrosis in atrial fibrillation', *Journal of Cardiovascular Magnetic Resonance,* 22(1), pp. 13.

Bui, A. H., Roujol, S., Foppa, M., Kissinger, K. V., Goddu, B., Hauser, T. H., Zimetbaum, P. J., Ngo, L. H., Manning, W. J., Nezafat, R. and Delling, F. N. (2017) 'Diffuse myocardial fibrosis in patients with mitral valve prolapse and ventricular arrhythmia', *Heart,* 103(3), pp. 204-209.

Cartoski, M. J., Nikolov, P. P., Prakosa, A., Boyle, P. M., Spevak, P. J. and Trayanova, N. A. (2019) 'Computational identification of ventricular arrhythmia risk in pediatric myocarditis', *Pediatr Cardiol,* 40(4), pp. 857-864.

Chu, L. C., Corona-Villalobos, C. P., Halushka, M. K., Zhang, Y., Pozzessere, C., Kamel, I. R., Pozios, I., Van Der Geest, R. J., Gai, N., Abraham, R. M., Abraham, T. P., Bluemke, D. A. and Zimmerman, S. L. (2017) 'Structural and functional correlates of myocardial T1 mapping in 321 patients with hypertrophic cardiomyopathy', *J Comput Assist Tomogr,* 41(4), pp. 653-660.

Coppini, R., Ferrantini, C., Yao, L., Fan, P., Del Lungo, M., Stillitano, F., Sartiani, L., Tosi, B., Suffredini, S., Tesi, C., Yacoub, M., Olivotto, I., Belardinelli, L., Poggesi, C., Cerbai, E. and Mugelli, A. (2013) 'Late sodium current inhibition reverses electromechanical dysfunction in human hypertrophic cardiomyopathy', *Circulation,* 127(5), pp. 575-584.

Ellims, A. H., Iles, L. M., Ling, L., Chong, B., Macciocca, I., Slavin, G. S., Hare, J. L., Kaye, D. M., Marasco, S. F., McLean, C. A., James, P. A., du Sart, D. and Taylor, A. J. (2014) 'A comprehensive evaluation of myocardial fibrosis in hypertrophic cardiomyopathy with cardiac magnetic resonance imaging: linking genotype with fibrotic phenotype', *Eur Heart J,* 15(10), pp. 1108-1116.

Ellims, A. H., Iles, L. M., Ling, L., Hare, J. L., Kaye, D. M. and Taylor, A. J. (2012) 'Diffuse myocardial fibrosis in hypertrophic cardiomyopathy can be identified by cardiovascular

magnetic resonance, and is associated with left ventricular diastolic dysfunction', *J Cardiovasc Magn Reson,* 14(1), pp. 76.
Galati, G., Leone, O., Pasquale, F., Olivotto, I., Biagini, E., Grigioni, F., Pilato, E., Lorenzini, M., Corti, B., Foà, A., Agostini, V., Cecchi, F. and Rapezzi, C. (2016) 'Histological and Histometric Characterization of Myocardial Fibrosis in End-Stage Hypertrophic Cardiomyopathy: A Clinical-Pathological Study of 30 Explanted Hearts', *Circ Heart Fail,* 9(9), pp. e003090.
Gersh, B. J., Maron, B. J., Bonow, R. O., Dearani, J. A., Fifer, M. A., Link, M. S., Naidu, S. S., Nishimura, R. A., Ommen, S. R., Rakowski, H., Seidman, C. E., Towbin, J. A., Udelson, J. E. and Yancy, C. W. (2011) 'American College of Cardiology Foundation/American Heart Association Task Force on Practice Guidelines. 2011 ACCF/AHA Guideline for the Diagnosis and Treatment of Hypertrophic Cardiomyopathy: a report of the American College of Cardiology Foundation/American Heart Association Task Force on Practice Guidelines. Developed in collaboration with the American Association for Thoracic Surgery, American Society of Echocardiography, American Society of Nuclear Cardiology, Heart Failure Society of America, Heart Rhythm Society, Society for Cardiovascular Angiography and Interventions, and Society of Thoracic Surgeons', *J Am Coll Cardiol,* 58(25), pp. e212-e260.
Iles, L., Pfluger, H., Phrommintikul, A., Cherayath, J., Aksit, P., Gupta, S. N., Kaye, D. M. and Taylor, A. J. (2008) 'Evaluation of diffuse myocardial fibrosis in heart failure with cardiac magnetic resonance contrast-enhanced T1 mapping', *J Am Coll Cardiol,* 52(19), pp. 1574-1580.
Jayatilleke, I., Doolan, A., Ingles, J., McGuire, M., Booth, V., Richmond, D. R. and Semsarian, C. (2004) 'Long-term follow-up of implantable cardioverter defibrillator therapy for hypertrophic cardiomyopathy', *American Journal of Cardiology,* 93(9), pp. 1192-1194.
Lambiase, P. D., Gold, M. R., Hood, M., Boersma, L., Theuns, D. A. M. J., Burke, M. C., Weiss, R., Russo, A. M., Kääb, S. and Knight, B. P. (2016) 'Evaluation of subcutaneous ICD early performance in hypertrophic cardiomyopathy from the pooled EFFORTLESS and IDE cohorts', *Heart Rhythm,* 13(5), pp. 1066-1074.
Maron, B. J. (2004) 'Hypertrophic cardiomyopathy: an important global disease', *Am J Med,* 116(1), pp. 63-63.
Mewton, N., Liu, C. Y., Croisille, P., Bluemke, D. and Lima, J. (2011) 'Assessment of myocardial fibrosis with cardiac magnetic resonance', *J Am Coll Cardiol,* 57(8), pp. 891-903.
Nakamori, S., Bui, A. H., Jang, J., El-Rewaidy, H. A., Kato, S., Ngo, L. H., Josephson, M. E., Manning, W. J. and Nezafat, R. (2018) 'Increased myocardial native T1 relaxation time in patients with nonischemic dilated cardiomyopathy with complex ventricular arrhythmia', *Journal of Magnetic Resonance Imaging,* 47(3), pp. 779-786.
O'Mahony, C., Jichi, F., Pavlou, M., Monserrat, L., Anastasakis, A., Rapezzi, C., Biagini, E., Gimeno, J. R., Limongelli, G., McKenna, W. J., Omar, R. Z. and Elliott, P. M. (2014) 'A novel clinical risk prediction model for sudden cardiac death in hypertrophic cardiomyopathy (HCM risk-SCD)', *Eur Heart J,* 35(30), pp. 2010-2020.
Olivotto, I., Cecchi, F., Poggesi, C. and Yacoub, M. H. (2012) 'Patterns of disease progression in hypertrophic cardiomyopathy: An individualized approach to clinical staging', *Circ Heart Fail,* 5(4), pp. 535-546.
O'Hara, T., Virág, L., Varró, A. and Rudy, Y. (2011) 'Simulation of the undiseased human cardiac ventricular action potential: model formulation and experimental validation', *PLoS Comput Biol,* 7(5), pp. e1002061.

586 Plank, G., Zhou, L., Greenstein, J., Cortassa, S., Winslow, R., O'Rourke, B. and Trayanova, N.
587 (2008) 'From mitochondrial ion channels to arrhythmias in the heart: computational techniques
588 to bridge the spatio-temporal scales', *Philos Trans A Math Phys Eng Sci,* 366(1879).
589 Prakosa, A., Arevalo, H. J., Deng, D., Boyle, P. M., Nikolov, P. P., Ashikaga, H., Blauer, J. J. E.,
590 Ghafoori, E., Park, C. J., Blake III, R. C., Han, F. T., MacLeod, R. S., Halperin, H. R., Callans,
591 D. J., Ranjan, R., Chrispin, J., Nazarian, S. and Trayanova, N. A. (2018) 'Personalized virtual-
592 heart technology for guiding the ablation of infarct-related ventricular tachycardia', *Nat Biomed*
593 *Eng,* 2, pp. 732-740.
594 Prakosa, A., Malamas, P., Zhang, S., Pashakhanloo, F., Arevalo, H., Herzka, D. A., Lardo, A.,
595 Halperin, H., McVeigh, E., Trayanova, N. and Vadakkumpadan, F. (2014) 'Methodology for
596 image-based reconstruction of ventricular geometry for patient-specific modeling of cardiac
597 electrophysiology', *Progress in Biophysics and Molecular Biology,* 115(2), pp. 226-234.
598 Prassl, A. J., Kickinger, F., Ahammer, H., Grau, V., Schneider, J. E., Hofer, E., Vigmond, E. J.,
599 Trayanova, N. A. and Plank, G. (2009) 'Automatically generated, anatomically accurate meshes
600 for cardiac electrophysiology problems', *IEEE Trans Biomed Eng,* 56(5), pp. 1318-1330.
601 Schinkel, A. F. L., Vriesendorp, P. A., Sijbrands, E. J. G., Jordaens, L. J. L. M., ten Cate, F. J. and
602 Michels, M. (2012) 'Outcome and complications after implantable cardioverter defibrillator
603 therapy in hypertrophic cardiomyopathy', *Circ Heart Fail,* 5, pp. 552-559.
604 Shade, J. K., Ali, R. L., Basile, D., Popescu, D., Akhtar, T., Marine, J. E., Spragg, D. D., Calkins,
605 H. and Trayanova, N. A. (2020a) 'Preprocedure Application of Machine Learning and
606 Mechanistic Simulations Predicts Likelihood of Paroxysmal Atrial Fibrillation Recurrence
607 Following Pulmonary Vein Isolation', *Circulation: Arrhythmia and Electrophysiology,* 13(7).
608 Shade, J. K., Cartoski, M. J., Nikolov, P., Prakosa, A., Doshi, A., Binka, E., Olivieri, L., Boyle, P.
609 M., Spevak, P. J. and Trayanova, N. A. (2020b) 'Ventricular arrhythmia risk prediction in
610 repaired tetralogy of fallot using personalized computational cardiac models', *Heart Rhythm,*
611 17(3), pp. 408-414.
612 Shade, J. K., Prakosa, A., Popescu, D. M., Yu, R., Okada, D. R., Chrispin, J. and Trayanova, N.
613 A. (2021) 'Predicting risk of sudden cardiac death in patients with cardiac sarcoidosis using
614 multimodality imaging and personalized heart modeling in a multivariable classifier', *Science*
615 *Advances,* 7(31), pp. eabi8020.
616 ten Tusscher, K. H. W. J. and Panfilov, A. V. (2006) 'Alternans and spiral breakup in a human
617 ventricular tissue model', *Am J Physiol Heart Circ Physiol,* 291(3), pp. H1088-H1100.
618 Vigmond, E., Weber dos Santos, R., Prassl, A., Deo, M. and Plank, G. (2008) 'Solvers for the
619 cardiac bidomain equations', *Prog Biophys Mol Biol,* 96(1-3), pp. 3-18.
620